Impaired Clearance of Apoptotic Cells Promotes Synergy between Atherogenesis and Autoimmune Disease

Tamar Aprahamian,[1,3] Ian Rifkin,[2] Ramon Bonegio,[2] Bénédicte Hugel,[4] Jean-Marie Freyssinet,[4] Kaori Sato,[1] John J. Castellot, Jr.,[3] and Kenneth Walsh[1,3]

[1]*Molecular Cardiology, Whitaker Cardiovascular Institute and* [2]*Renal Section, Department of Medicine, Boston University School of Medicine, Boston, MA 02118*

[3]*Department of Anatomy and Cellular Biology, Program in Cellular, Molecular, and Developmental Biology, Tufts University School of Medicine, Boston, MA 02111*

[4]*Institut d'Hématologie et d'Immunologie, Faculté de Médecine, Université Louis Pasteur, 67085 Strasbourg et Institut National de la Santé et de la Recherche Médicale, U143, 94276 Le Kremlin-Bicetre, France*

Abstract

To clarify the link between autoimmune disease and hypercholesterolemia, we created the *gld.apoE*$^{-/-}$ mouse as a model of accelerated atherosclerosis. Atherosclerotic lesion area was significantly increased in *gld.apoE*$^{-/-}$ mice compared with *apoE*$^{-/-}$ mice. *gld.apoE*$^{-/-}$ mice also displayed increases in lymphadenopathy, splenomegaly, and autoantibodies compared with *gld* mice, and these effects were exacerbated by high cholesterol diet. *gld.apoE*$^{-/-}$ mice exhibited higher levels of apoptotic cells, yet a reduced frequency of engulfed apoptotic nuclei within macrophages. Infusion of lysophosphatidylcholine, a component of oxidized low density lipoprotein, markedly decreased apoptotic cell clearance in *gld* mice, indicating that hypercholesterolemia promotes autoimmune disease in this background. These data suggest that defects in apoptotic cell clearance promote synergy between atherosclerotic and autoimmune diseases.

Key words: atherosclerosis • autoimmunity • macrophages • lysophosphatidylcholine • lymphoproliferation

Introduction

Autoimmune disorders are characterized by the loss of tolerance to self-antigen and the consequent production of immunoglobulin G autoantibodies (1). The development of autoimmune disease involves a poorly understood interplay of genetic and environmental factors. Recently, it has been found that failure to degrade chromatin or properly clear apoptotic cells contributes to the development of autoimmunity. Impaired apoptotic debris clearance leads to the development of an autoimmune phenotype in mouse models (2, 3). Similarly, in humans, C1q and DNaseI deficiencies are associated with the development of SLE (4, 5), and apoptotic bodies and circulating DNA fragments are found in the sera of patients with SLE (6, 7). Furthermore, macrophages from patients with SLE display abnormal morphology and are impaired in their ability to clear apoptotic bodies (8).

Inflammatory cell activity plays an important role in the progression of atherosclerosis. Atherosclerotic lesions are initiated by injury to the endothelium by oxidized low density lipoprotein (oxLDL), inflammatory cytokines, and immune complexes, and its progression involves inflammatory cell interactions with the endothelium and extravasation into the subendothelial space (9). Several lines of genetic evidence in apolipoprotein E–deficient (*apoE*$^{-/-}$) or low density lipoprotein receptor-deficient mice suggest that both lymphocytes and macrophages contribute to the early and late stages of atherosclerotic lesion formation (10). Patients with autoimmune diseases, including SLE and rheumatoid arthritis, exhibit a higher incidence of atherosclerosis and are at significant risk of premature cardiovascular disease (11–15). There is considerable controversy regarding the causes of atherosclerosis in patients with autoimmune disease, although chronic inflammation is likely to be a contributing factor. Progress in understanding the mechanisms of accelerated atherosclerosis asso-

Address correspondence to Kenneth Walsh, Molecular Cardiology, Whitaker Cardiovascular Institute, Boston University School of Medicine, 715 Albany St., W611, Boston, MA 02118. Phone: (617) 414-2392; Fax: (617) 414-2391; email: kwalsh@world.std.com

Abbreviations used in this paper: aCL, anticardiolipin antibody; ANA, antinuclear antibody; LDL, low density lipoprotein; LPC, lysophosphatidylcholine; oxLDL, oxidized LDL; TUNEL, TdT-mediated dUTP nick-end labeling; VLDL, very LDL.

 J. Exp. Med. © The Rockefeller University Press • 0022-1007/2004/04/1121/11 $8.00
Volume 199, Number 8, April 19, 2004 1121–1131
http://www.jem.org/cgi/doi/10.1084/jem.20031557

ciated with autoimmune disease has been impaired by the lack of an appropriate animal model.

Fas is a receptor that initiates an apoptotic signal when bound to its ligand, FasL (16). Fas-mediated apoptosis functions in part to control peripheral lymphoid responses (17) and macrophage survival (18, 19). In humans, diminished Fas-mediated apoptosis gives rise to Canale-Smith syndrome, a disease associated with lymphoproliferation and autoimmunity (20–22). The *gld* and *lpr* mouse strains have inactivating mutations in FasL and Fas, respectively, and they suffer from lupuslike autoimmune disorders with autoantibody specificities similar to those seen with the human disease (23–26). In addition, they exhibit lymphadenopathy and splenomegaly. These mice typically do not exhibit signs of atherosclerosis, but they are susceptible to atherosclerotic lesion formation when fed an atherogenic diet containing cholic acid (27).

To develop a better understanding of the link between atherogenesis and autoimmune disease, we generated an atherosclerotic mouse model that lacks functional FasL by crossing $apoE^{-/-}$ with *gld* mice. The *gld*.$apoE^{-/-}$ mice displayed enhanced atherosclerosis compared with $apoE^{-/-}$ mice reminiscent of accelerated atherosclerosis seen in patients with autoimmune disease. These mice also exhibited increased lymphoproliferation and autoimmunity compared with *gld* mice, and this phenotype was enhanced by a high-fat diet. The *gld*.$apoE^{-/-}$ mice had high levels of apoptotic material both in tissues and in the circulation. This was due, at least in part, to an impaired ability to scavenge apoptotic debris, suggesting that synergism between atherosclerosis and autoimmune disease can be mediated by impaired apoptotic body clearance.

Materials and Methods

Generation of Mice and Study Protocol. $apoE^{-/-}$ and *gld* mice were obtained from Jackson ImmunoResearch Laboratories on the C57BL/6J background. The *gld* mutation is a point mutation in the FasL gene that occurred spontaneously in the C3H/HeJ strain (24). Fully congenic C57/B6-*gld* mice have been generated by transferring the *gld* mutation to the C57BL/6J background for 10 generations of backcrossing. Single knockout mice were interbred to produce homozygous groups of mice with the following genotypes: $apoE^{-/-}$, *gld*, *gld*.$apoE^{-/-}$, and $apoE^{+/+}gld^{+/+}$ (WT). Mice were maintained on a Purina ProLab 3000 mouse diet (Normal Diet), and at 7 wk of age, mice from each genotype received either normal diet or Teklad adjusted calories Western diet: 21% (weight/weight) fat, 0.15% (weight/weight) cholesterol, and 19.5% (weight/weight) casein, without sodium cholate. All mouse experiments were performed under protocols approved by the Institutional Animal Care and Use Committee of Boston University School of Medicine.

PCR Analysis for ApoE Genotype. The *apoE* genotype was determined by PCR analysis using DNA extracted from tail samples (QIAGEN). The *apoE* alleles were detected using three primers that produced 155-bp or 245-bp products, respectively. The apoE primers were as follows: 5′-GCCTAGCCGAGGGAGAGCCG-3′ and 5′-TGTGACTTGGGAGCTCTGCAGC-3′ for the wild-type allele and 5′-GCCGCCCCGACTGCATCT-3′ for the deficient allele.

Gld Mutation Detection by Fluorescent Sequencing. The *gld*-derived progeny were genotyped by sequence analysis. A 437-bp PCR fragment was generated with primers GLDF1, 5′-AACCCCCACTCAAGGTCCATCCCTCTG-3′, and GLDR0, 5′-ATATTCCTGGTGCCCATGAT-3′. The PCR products were labeled using the PE BigDye Terminator Cycle Sequencing Ready Reaction Kit (Applied Biosystems), and sequenced. The area of interest was ~100 bp downstream from the start of the amplified fragment. In this region, the sequence 5′-CCTTTTT-3′ indicated the wild-type *FasL* allele, whereas 5′-CCCTTTT-3′ indicated *gld* and 5′-CC(C/T)TTTT-3′ indicated a heterozygote (unpublished data).

Quantitative Analyses of Atherosclerosis, Hyperlipidemia, Splenomegaly, and Lymphadenopathy. After 12 wk on a Western or normal diet, food was removed for an 8-h fast. After the fast, the mice were weighed and sacrificed. Blood was drawn by cardiac puncture for determination of total plasma cholesterol and triglyceride levels (Excell Labs). Heart, spleen, and submandibular lymph nodes were excised and weighed. The vasculature was perfused intracardially with 0.9% sodium chloride, and the aorta was isolated from the aortic arch to the iliac bifurcation. The adventitia was thoroughly stripped, and the aorta opened longitudinally, pinned to a white silicone gel, and fixed in 10% neutral buffered formalin for 24 h. After fixation, aortae were rinsed with PBS, stained with Oil red O solution, and destained in 60% isopropyl alcohol. Aortae were photographed using an Olympus digital camera, and lesion size was measured using a National Institutes of Health image program on a Macintosh computer. Because there was no significant difference in lesion area between males and females (unpublished data), datasets for both sexes were combined.

Cell Isolation and Flow Cytometry. Lymph nodes were harvested, minced, and put through a 70-μm cell strainer. Cells were washed in 2% FBS/PBS and stained for 15 min at 4°C. Flow cytometry analysis was performed using fluorescence-labeled monoclonal antibodies against the following: CD3-CyC, CD4-FITC, CD8-PE (BD Biosciences), or TdT-mediated dUTP nick-end labeling (TUNEL; Roche Diagnostics Corp.).

Immunohistochemistry. Aortae were fixed using 10% neutral buffered formalin and paraffin embedded. 6-μm sections of aorta were cut from the aortic arch to the thoracic aorta. Slides were deparaffinized, treated with 3% hydrogen peroxide for 30 min, and blocked in 10% goat serum using an avidin/biotin block. Samples were incubated overnight at 4°C in rat anti–mouse F4/80 (dilution 1:40; Serotec, Inc.), rat anti–mouse CD3 (dilution 1:1,000; BD Biosciences), or mouse IgG as a negative control in 5% goat serum/PBS. After washing, samples were incubated for 30 min in goat anti–rat IgG diluted 1:500 (Caltag). Visualization of immune complexes with streptavidin–horseradish peroxidase and aminoethylcarbazole was followed by a hematoxylin counterstain. Macrophage and T cell quantification were determined by scoring samples from at least eight mice per group, choosing every sixth slide from the aortic arch through the thoracic aorta. Analysis was performed by two investigators who were blinded to the sample identity. Lymph nodes were fixed and sectioned according to the aforementioned protocol. TUNEL staining was performed according to the manufacturer's directions (Roche Diagnostics Corp.). Quantification of all TUNEL staining was performed by examining six randomly selected fields in each lymph node section by two investigators who were blinded to sample identity. To generate the overlapping merged figures, sequential sections were used for fluorescent staining of macrophages and follicular dendritic cells with anti–mouse F4/80 (Caltag) and anti–mouse CD21 (BD Biosciences). Macrophage

ingestion of TUNEL-positive apoptotic debris was quantified as described previously (3).

Autoantibodies. Serum levels of antinuclear antibodies (ANAs) were measured by immunofluorescence using Hep-2–coated slides (The Binding Site Inc.). Slides were incubated for 20 min with serial dilutions (1:40 to 1:2,560) of mouse serum in PBS, washed in PBS, and incubated with FITC-labeled goat anti–mouse IgG (whole molecule; Sigma-Aldrich). Slides were counterstained with Evan's blue and viewed using fluorescent microscopy. The titer value is defined as the inverse value of the last positive dilution. Anticardiolipin antibodies were measured using a commercially available ELISA assay that detected IgG (Alpha Diagnostic). Values are reported as the mean absorbance. Serum IgG levels were measured using a commercially available ELISA assay (Bethyl Laboratories).

Kidney Analysis. Urine samples were obtained using metabolic cages from 19-wk-old wild-type, apoE$^{-/-}$, *gld*, and *gld.apoE*$^{-/-}$ mice maintained on normal diet. Samples were diluted 1:10 and measured using a protein assay (Bio-Rad Laboratories) at an absorbance of 595 nm. Calculations are shown as milligrams of protein per 24 h. Formalin-fixed kidney sections were stained with hematoxylin and eosin. Stained sections were coded, digitally photographed, and analyzed by an investigator who was blinded to section identity using a stereo microscope (Nikon) fitted with a digital camera (Diagnostic Instruments). Glomerular cross-sectional areas of at least 25 glomeruli from five randomly photographed low-powered fields were measured in each animal using computer-assisted pixel counting (Photopaint 10; Corel Corporation). Mean glomerular tuft area (A_G) for each animal was calculated from all available glomerular profiles, and tuft volume (V_G) was calculated as well (28). $V_G = (B/k)(A_G)^{1.5}$ where B is the shape coefficient for an idealized glomerulus (B = 1.38) and k is a size distribution coefficient (k = 1.10).

Serum Microparticles. Platelet-free plasma was isolated and analyzed as described previously (29). In brief, whole blood was mixed with 0.138 M sodium citrate and centrifuged. After retrieval of the plasma, microparticle concentration was determined by capture onto insolubilized annexin V and reported as the nanomolar concentration of phosphatidylserine equivalents.

Intravenous Infusion. 6-mo-old wild-type or *gld* mice were anesthetized with an intraperitoneal injection of sodium pentobarbital and maintained with supplementary doses as needed. A catheter was inserted into the tail vein for the intravenous infusion of freshly prepared lysophosphatidylcholine (LPC) at rates of 1.5 or 3 pmol/min. Body temperature was maintained by a heating pad. Mice were killed 120 min after the start of infusion. Lymph nodes were harvested, fixed in 10% formalin, and processed for TUNEL staining as described previously.

Statistical Analysis. Results are shown as the mean ± SEM. Differences between groups were determined by analysis of variance and Student's *t* test using the InStat program and were considered statistically significant for $P < 0.05$.

Results

Lack of FasL in apoE$^{-/-}$ Mice Leads to Greater Atherosclerotic Lesion Area. The aortae of *gld.apoE*$^{-/-}$ and *apoE*$^{-/-}$ mice maintained on a 12-wk Western diet demonstrated grossly visible atherosclerotic lesions after Oil red O staining. Lesion area in the *apoE*$^{-/-}$ mice in this work was in agreement with previously described values (30). Considerably greater lesion area was present in the *gld.apoE*$^{-/-}$ mice compared with *apoE*$^{-/-}$ throughout the length of the aorta (Fig. 1 a). Image analysis revealed a threefold increase in plaque area in the aorta of the *gld.apoE*$^{-/-}$ mice compared with *apoE*$^{-/-}$ (27.9 ± 2.84 mm^2 and 9.10 ± 0.9 mm^2, respectively; $P < 0.001$) (Fig. 1 c). Lesion area analyses were also performed on age-matched mice that were maintained on normal diet (Fig. 1 b). Again, *gld.apoE*$^{-/-}$ mice had significantly larger amounts of lesion area when compared with *apoE*$^{-/-}$: 6.7 ± 0.5 mm^2 and 2.1 ± 0.3 mm^2, respectively ($P < 0.001$) (Fig. 1 c). In contrast, *gld* and wild-type mice had virtually no detectable lesions on either Western or normal diet.

Inflammation and Apoptotic Bodies in Vascular Lesions. Histological analysis of aortae of *gld* and wild-type mice with the macrophage marker F4/80 or the T cell marker CD3 revealed no evidence of macrophage or T cell infiltration (unpublished data), which was consistent with the lack of visible lesions within these vessels. In contrast, the aortae of *gld.apoE*$^{-/-}$ and *apoE*$^{-/-}$ displayed evidence of macrophage and T cell extravasation within lesions (Fig. 2, a, b, d, and e). Quantitative analyses revealed approximately threefold more macrophage staining in the vessel cross-sections from the *gld.apoE*$^{-/-}$ than the *apoE*$^{-/-}$ mice (Fig. 2 c). Examination of T cells revealed a similar result, showing an increase in T cells within the lesions in the *gld.apoE*$^{-/-}$ mice relative to the *apoE*$^{-/-}$ mice (Fig. 2 f). TUNEL immunofluorescence staining of vessel segments revealed apoptotic cells within the atherosclerotic lesions of the *apoE*$^{-/-}$ mice that can be distinguished from the background autofluorescence of the elastic lamina (Fig. 2 g).

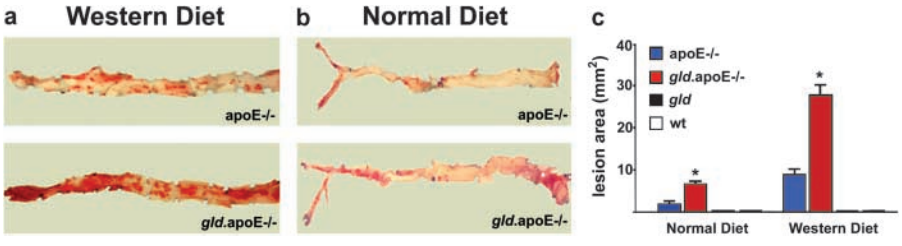

Figure 1. Atherosclerotic lesions in the aortae of *gld.apoE*$^{-/-}$ and *apoE*$^{-/-}$ mice are visualized by Oil red O staining. The increase in atherosclerotic lesion area of the *gld.apoE*$^{-/-}$, compared with the *apoE*$^{-/-}$, is macroscopically visible on (a) Western diet, as well as (b) normal diet. The *gld* and wild-type mice showed no visible lesions (not depicted). (c) Quantification of Oil red O staining area revealed a statistically significant increase in lesion size on Western diet of the *gld.apoE*$^{-/-}$ ($n = 26$) compared with the *apoE*$^{-/-}$ ($n = 27$), and normal diet *gld.apoE*$^{-/-}$ ($n = 11$) compared with the *apoE*$^{-/-}$ ($n = 8$) (*, $P < 0.001$ vs. *apoE*$^{-/-}$).

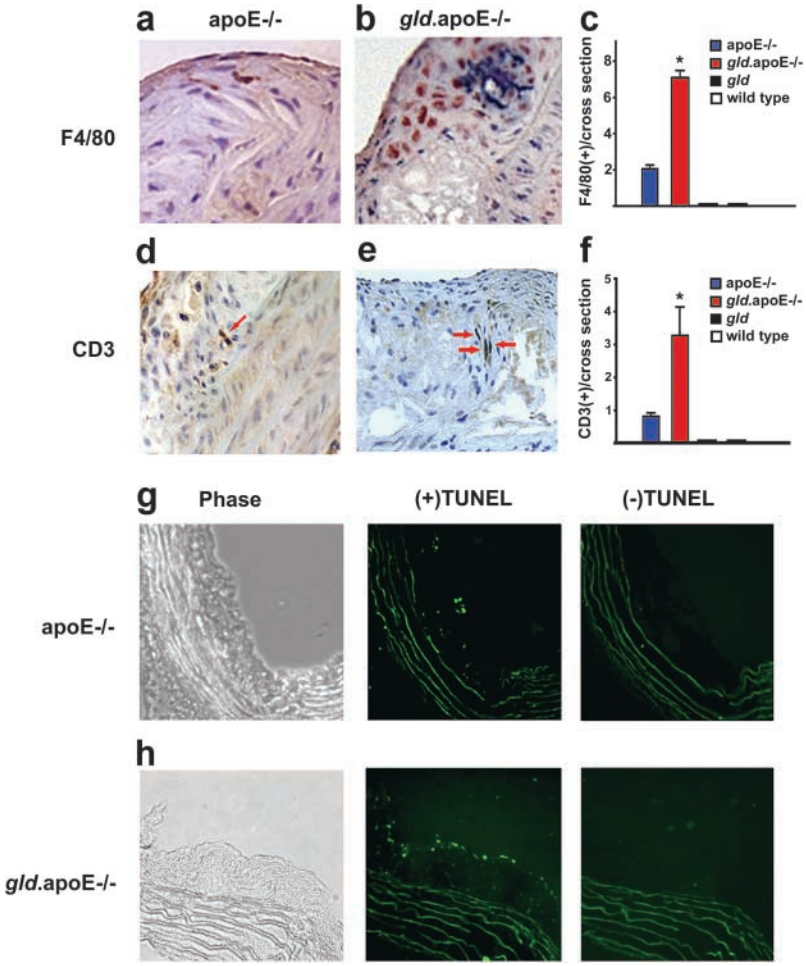

Figure 2. Vessel wall inflammation is increased in *gld.apoE*$^{-/-}$ mice compared with *apoE*$^{-/-}$ mice. Representative sections of atherosclerotic lesions from the aortic arch of the *gld.apoE*$^{-/-}$ and *apoE*$^{-/-}$ mice, maintained on a Western diet for 12 wk. Specimens were stained with F4/80 for macrophages, or (d and e) CD3 for T cells, represented by the brown staining (arrows). The increase of macrophages and T cells is quantified in c and f, respectively. Macrophages and T cell content were significantly higher in the lesions of *gld.apoE*$^{-/-}$ mice ($n = 11$) compared with *apoE*$^{-/-}$ ($n = 10$) (*, $P < 0.001$ vs. *apoE*$^{-/-}$). (g) Representative photomicrograph of TUNEL staining in lesions of *apoE*$^{-/-}$ mice. (h) Representative photomicrograph of TUNEL staining in lesions of *gld-apoE*$^{-/-}$ mice showing a greater amount of TUNEL-positive fragments than in the *apoE*$^{-/-}$ lesions. The (−)TUNEL condition indicates sections processed without the terminal deoxynucleotidyl transferase enzyme to assess background autofluorescence of the elastic lamina.

The frequency of TUNEL-positive cells in these lesions was low, consistent with a previous paper (31). In contrast, markedly higher levels of TUNEL-positive fragments were apparent in the vessel wall lesions of the *gld.apoE*$^{-/-}$ mice (Fig. 2 h). Apoptotic debris typically localized near the lumenal surface of the vessel wall, although some positive staining was present within the lesion.

FasL Deficiency Reduces Cholesterol Levels in apoE-deficient Mice. Total plasma cholesterol was determined for all groups of mice on both Western diet and normal diet (Fig. 3 a). Although the *gld.apoE*$^{-/-}$ mice became hypercholesterolemic on Western diet, the extent of hypercholesterolemia was less than that of *apoE*$^{-/-}$ mice. There was also a trend toward lower cholesterol levels in the *gld.apoE*$^{-/-}$ relative to the *apoE*$^{-/-}$ in the mice fed normal diet, but this was not statistically significant. With either diet, the *gld* mice had lipid plasma levels similar to the wild-type controls. Compared with control mice, *apoE*$^{-/-}$ mice showed a mild increase in plasma triglyceride levels when fed Western diet and normal diet, consistent with previous papers (30) as did the *gld.apoE*$^{-/-}$ (unpublished data). Fast performance liquid chromatography on each of the four experimental groups was performed on pooled serum samples. The *gld.apoE*$^{-/-}$ and *apoE*$^{-/-}$ had profiles containing higher very low density lipoprotein (VLDL) and low density lipoprotein (LDL) levels, and low high density lipoprotein levels compared with the *gld* and the wild-type mice (Fig. 3 b and not depicted). VLDL levels were lower in *gld.apoE*$^{-/-}$mice compared with *apoE*$^{-/-}$ mice. There was no significant difference in lipid profile between the *gld* and the wild-type mouse on normal diet and Western diet (unpublished data).

Lack of apoE Exacerbates gld Phenotype. At the time of killing, body weight and heart weight showed little or no difference in the four strains of mice (unpublished data). In contrast, spleen and lymph nodes from *gld* and *gld.apoE*$^{-/-}$ mice showed remarkable increases in weight and size. Although enlargement of these two organs is a characteristic of the *gld* phenotype, the spleen and lymph nodes of *gld.apoE*$^{-/-}$ mice were significantly larger when compared with their *gld* counterparts (Fig. 4, a and b). Spleen weight of *gld.apoE*$^{-/-}$ mice increased to almost double that found for *gld* in animals fed a Western diet (0.75 ± 0.07 g vs. 0.34 ± 0.05 g; $P < 0.001$), and approximately fivefold that found in wild-type or *apoE*$^{-/-}$ mice (Fig. 4 c). This trend in spleen size was also observed for these strains when maintained on normal diet: 0.33 ± 0.05 g for *gld.apoE*$^{-/-}$ and 0.25 ± 0.03 g for *gld* ($P < 0.05$). Quantification of the submandibular lymph nodes also revealed a

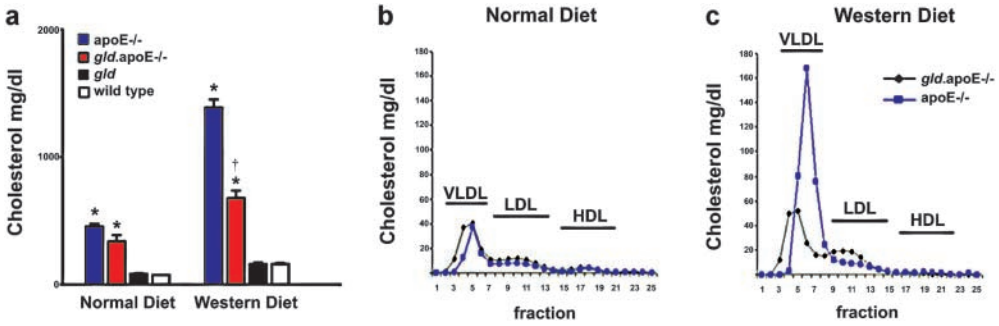

Figure 3. Lipid profiles of $apoE^{-/-}$ and $gld.apoE^{-/-}$ mice maintained on normal diet and Western diet. (a) Total cholesterol levels were determined in $gld.apoE^{-/-}$ ($n = 32$), $apoE^{-/-}$ ($n = 31$), *gld* ($n = 26$), and wild type ($n = 31$) on Western diet and in $gld.apoE^{-/-}$ ($n = 11$), $apoE^{-/-}$ ($n = 8$), *gld* ($n = 5$), and wild type ($n = 5$) on normal diet (*, $P < 0.001$ vs. *gld*, wild type; †, $P < 0.001$ vs. $apoE^{-/-}$). (b) Fast performance liquid chromatography profiles of sera from $gld.apoE^{-/-}$ and $apoE^{-/-}$ mice maintained on normal and Western diet. VLDL, LDL, and high density lipoprotein fraction locations are indicated.

statistically significant increase in weight comparing the $gld.apoE^{-/-}$ with the *gld*: 0.07 ± 0.02 g for wild type versus 0.1 ± 0.002 g for $apoE^{-/-}$, and 0.40 ± 0.07 g for *gld* versus 1.05 ± 0.08 g for $gld.apoE^{-/-}$ ($P < 0.001$) when maintained on a high-cholesterol Western diet (Fig. 4 d). Likewise, a similar pattern was observed for mice maintained on normal diet.

$CD4^+$ T cells are important for autoantibody production and the pathogenesis of autoimmunity, and the lymphoproliferation seen in Fas or FasL-deficient mice and humans is due predominantly to the expansion of an unusual T cell population that is $CD3^+$, but lacks both CD4 and CD8 (double negative T cells; reference 32). We performed a phenotypic analysis of lymph node T cells from *gld* and $gld.apoE^{-/-}$ mice to determine whether the enhanced lymphoproliferation and autoimmunity seen in the $gld.apoE^{-/-}$ mice could be accounted for by obvious alterations in the ratio of the different T cell subsets (Table I). No significant differences in percentages of $CD4^+$, $CD8^+$, or double negative $CD3^+CD4^-CD8^-$ T cells were seen. The total number of all T cell subsets was increased in the $gld.apoE^{-/-}$ mice (unpublished data), reflecting their larger lymph node

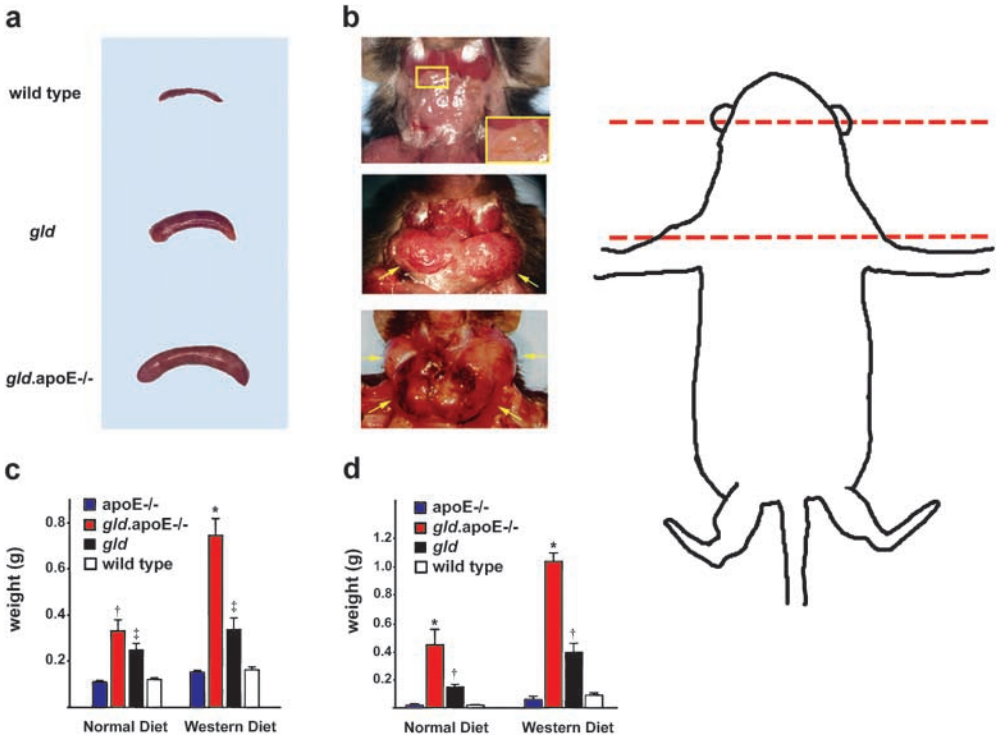

Figure 4. Lymphadenopathy and splenomegaly in *gld* and $gld.apoE^{-/-}$ mice. (a) Representative spleens excised from paired littermates of wild-type, *gld*, and $gld.apoE^{-/-}$ mice. (b) Representative submandibular lymph nodes (arrows) dissected from paired littermates of wild-type, *gld*, and $gld.apoE^{-/-}$ mice. Inset shows higher magnification image of lymph node from wild-type mouse. Diagram illustrates dissected area. (c) Spleen weights in the different strains of mice fed normal diet: $gld.apoE^{-/-}$ ($n = 11$), $apoE^{-/-}$ ($n = 8$), *gld* ($n = 5$), and wild type ($n = 5$); or Western diet: $gld.apoE^{-/-}$ ($n = 26$), $apoE^{-/-}$ ($n = 31$), *gld* ($n = 26$), and wild type ($n = 31$) (*, $P < 0.001$ vs. *gld*; †, $P < 0.05$ vs. *gld*; ‡, $P < 0.001$ vs. $apoE^{-/-}$, wild type). (d) Lymph node weights in the different strains of mice fed normal diet: $gld.apoE^{-/-}$ ($n = 11$), $apoE^{-/-}$ ($n = 8$), *gld* ($n = 5$), and wild type ($n = 5$); or Western diet: $gld.apoE^{-/-}$ ($n = 26$), $apoE^{-/-}$ ($n = 31$), *gld* ($n = 26$), and wild type ($n = 31$) (*, $P < 0.001$ vs. *gld*; †, $P < 0.001$ vs. $apoE^{-/-}$, wild type).

Table I. *Percent T Cell Composition of Lymph Nodes*

	$CD4^+$	$CD8^+$	$CD3^+CD4^-CD8^-$
gld	13.0 ± 4.8	5.9 ± 2.1	43.3 ± 9.7
gld.apoE$^{-/-}$	16.4 ± 4.1	7.7 ± 3.6	33.5 ± 11.2

size, which was most likely due to an overall enhancement of the autoimmune process in these mice.

ANAs, the prototypic autoantibodies in SLE, were assessed in the different lines of mice maintained on normal diet or Western diets. As expected, wild-type and *apoE*$^{-/-}$ mice showed no evidence of ANAs, whereas *gld* mice exhibited high titers on normal diet and Western diet (Table II). ANA titers in *gld.apoE*$^{-/-}$ were significantly elevated compared with the *gld* mice on normal diet, and titers were further elevated by Western diet. Serum levels of anticardiolipin antibody (aCL) were modestly enhanced in *apoE*$^{-/-}$ mice compared with wild-type, which was consistent with a previous paper (33), and these levels were further elevated by Western diet (Table II). The levels of aCL were higher in *gld* mice than in *apoE*$^{-/-}$ mice and the Western diet led to a further elevation of aCL in *gld* mice. The *gld.apoE*$^{-/-}$ mice displayed the highest levels of aCL, which were approximately fourfold higher than that seen in *gld* mice on either normal or Western diets. The *gld.apoE*$^{-/-}$ mice also displayed elevated levels of IgG on both normal and Western diet, indicative of a polyclonal B cell activation (Table II).

Because autoimmune disease is frequently associated with renal dysfunction, a histological analysis was performed on the kidneys from the four strains of mice. Kidneys from *gld.apoE*$^{-/-}$ mice had larger, more cellular glomeruli compared with all other strains (Fig. 5 a). Quantification revealed that, whereas the wild-type, *apoE*$^{-/-}$, and *gld* mice had glomerular tuft volumes of 1.6×10^6 μm^3, 1.3×10^6 μm^3, and 2.1×10^6 μm^3, respectively, the *gld.apoE*$^{-/-}$ volumes were significantly increased to 5.0×10^6 μm^3 (Fig. 5 b). Correspondingly, proteinuria was observed in the *gld.apoE*$^{-/-}$ mice (Fig. 5 c), a further indication of renal impairment.

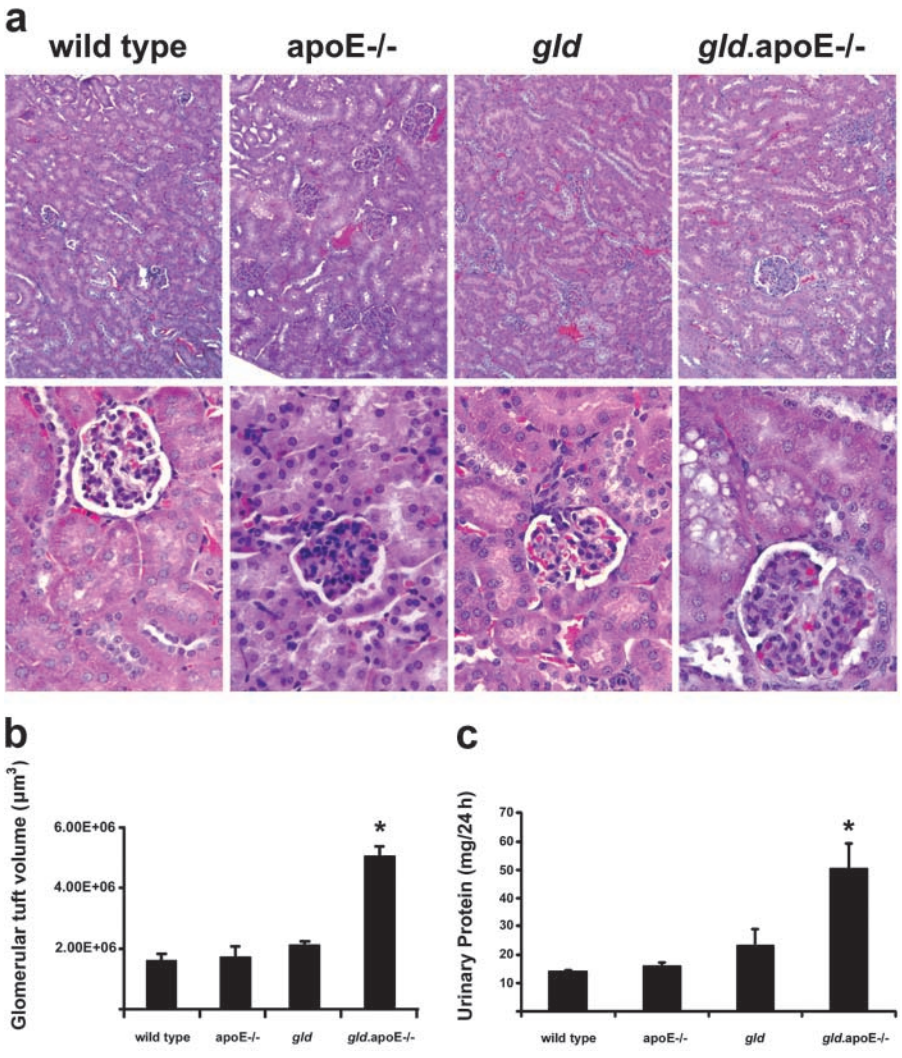

Figure 5. Evidence of renal dysfunction in the *gld.apoE*$^{-/-}$ mouse. (a) Representative hematoxylin and eosin stained sections of renal tissue showing typical glomeruli in *gld.apoE*$^{-/-}$ mice compared with wild-type, *apoE*$^{-/-}$, and *gld* mice when maintained on Western diet. (top) Magnification, 100. (bottom) Magnification, 400. (b) Quantification of glomerular tuft volume revealed a statistically significant increase in glomerular size in the *gld.apoE*$^{-/-}$ mice compared with the control groups (*, $P < 0.001$). (c) The output of urinary protein by *gld.apoE*$^{-/-}$ mice maintained on normal diet was significantly increased compared with wild type, *apoE*$^{-/-}$, and *gld* (*, $P < 0.001$).

Table II. *Circulating Autoantibody Levels*

	ANA (titer)[a]		aCL		Serum IgG	
	Normal diet	Western diet	Normal diet	Western diet	Normal diet	Western diet
			A	*A*	*mg/ml*	*mg/ml*
WT	ND	ND	0.056 ± 0.03	0.067 ± 0.04	0.79 ± 0.60	0.61 ± 0.06
apoE$^{-/-}$	ND	ND	0.084 ± 0.02	0.154 ± 0.06	0.02 ± 0.57	0.77 ± 0.17
gld	104 ± 24	120 ± 25	0.164 ± 0.02	0.193 ± 0.03	0.19 ± 0.59	1.79 ± 0.51
gld.apoE$^{-/-}$	400 ± 80[b]	823 ± 118[b,c]	0.658 ± 0.16[b]	0.859 ± 0.31[b]	5.53 ± 2.85[d]	4.25 ± 0.72[d]

[a]Inverse titer of last positive dilution.
[b]$P < 0.001$ versus WT, *apoE*$^{-/-}$, *gld*.
[c]$P < 0.05$ versus *gld.apoE*$^{-/-}$ on normal diet.
[d]$P < 0.01$ versus WT, *apoE*$^{-/-}$, *gld*.
A, absorbance; aCL, anticardiolipin; ANA, antinuclear antibody.

Increased Apoptotic Material and Impaired Clearance in gld.apoE$^{-/-}$ *Mice.* Apoptotic material was analyzed in the sera and lymph nodes of the different groups of mice. Apoptotic fragments within the lymph nodes were visualized using TUNEL immunofluorescent staining. Very few TUNEL-positive fragments were observed in the wild-type and *apoE*$^{-/-}$ mice (Fig. 6 a and not depicted). The *gld* mice showed an increase in the frequency of TUNEL-positive fragments compared with wild-type or *apoE*$^{-/-}$ (Fig. 6 b). However, the frequency of TUNEL-positive fragments was 40% higher in the *gld.apoE*$^{-/-}$ mice than in the *gld* ($P < 0.01$), and higher levels of apoptotic nuclei were seen when *gld.apoE*$^{-/-}$ mice were fed a Western diet ($P < 0.05$) (Fig. 6, c and d). These histological results were corroborated by FACS® analysis of TUNEL-positive fragments (Fig. 6 e).

A microparticle analysis was performed on platelet-free plasma using annexin V capture to assess the levels of apoptotic microparticles in the circulation (29). Although the differences between experimental groups was not as strik-

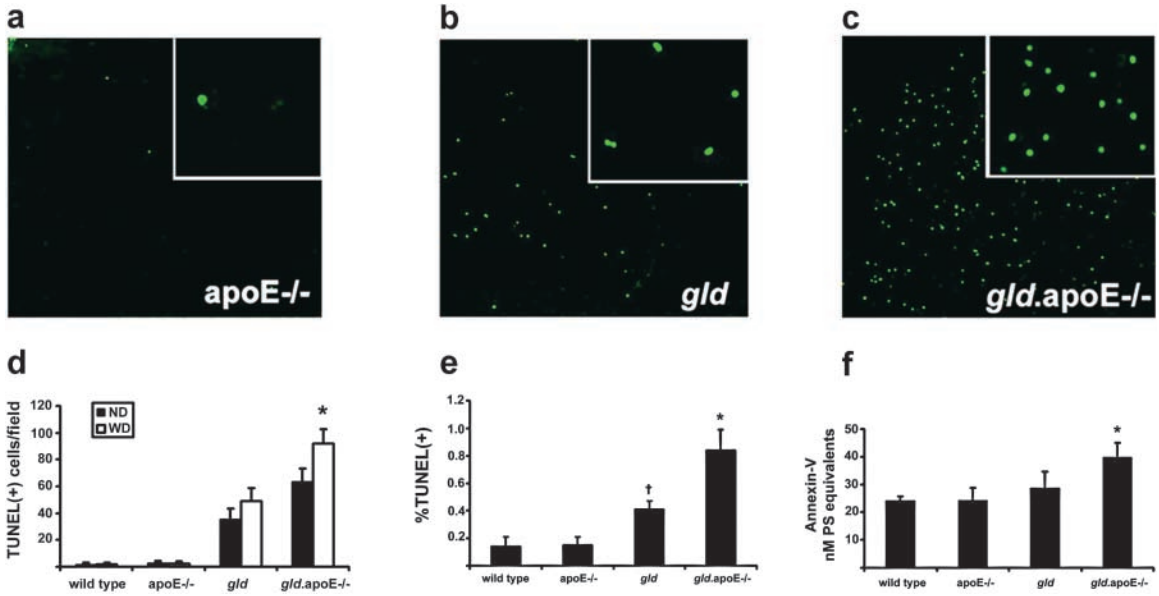

Figure 6. Elevated apoptotic fragments in lymph node and circulation of *gld.apoE*$^{-/-}$ mice. (a–c) Lymph node sections from animals fed Western diet were stained with TUNEL (FITC) and (d) quantified showing number of TUNEL-positive cells in the different strains of mice maintained on normal or Western diet (*, $P < 0.05$ vs. *gld.apoE*$^{-/-}$ on normal diet). *gld.apoE*$^{-/-}$ also showed a significant increase in TUNEL-positive cells compared with *gld* mice on normal or Western diet, respectively. Insets in a–c show higher magnification views. (e) FACS® analysis of TUNEL-positive cells in freshly isolated lymph node from Western diet–fed mice corroborates the histological findings (*, $P < 0.05$ vs. *gld*; $P < 0.01$ vs. WT, *apoE*$^{-/-}$; †, $P < 0.05$ vs. WT, *apoE*$^{-/-}$). (f) Platelet-free plasma isolated from different strains of mice on Western diet and assayed for apoptotic fragments by annexin V capture (*, $P < 0.05$ vs. *gld*; $P < 0.01$ vs. WT, *apoE*$^{-/-}$).

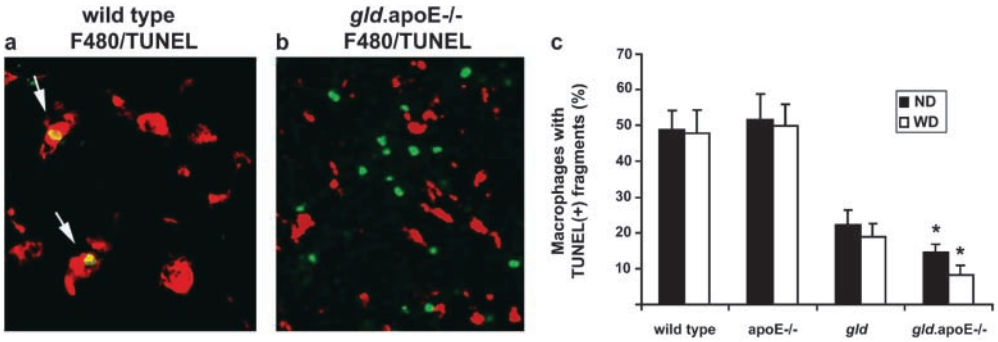

Figure 7. Evidence of impaired macrophage function in *gld.apoE*$^{-/-}$ mice. (a) Lymph node sections of wild-type mice stained with TUNEL (FITC) and F480 (PE) show colocalization of TUNEL-positive cells and macrophages (arrows, yellow merge). (b) Lymph node sections of *gld.apoE*$^{-/-}$ mice stained with TUNEL (FITC) and F480 (PE) show an abnormal morphology of macrophages and diminished colocalization. (c) Quantified results revealing a statistically significant decrease of macrophage ingestion of TUNEL-positive fragments in the *gld* and *gld.apoE*$^{-/-}$ mice, with *gld.apoE*$^{-/-}$ mice decreasing further than *gld* on both normal diet and Western diet (*, $P < 0.05$ vs. *gld*).

ing as that found with TUNEL analyses of lymph node sections, the *gld.apoE*$^{-/-}$ mice showed significant increase in total microparticle concentration, relative to wild-type and *apoE*$^{-/-}$ mice (Fig. 6 f). The microparticle population in *gld.apoE*$^{-/-}$ mice was >30% endothelial origin based on an anti-CD31 colocalization procedure (reference 29 and unpublished data).

Further histological analyses of lymph node sections from *gld.apoE*$^{-/-}$ mice were performed to assess the uptake of apoptotic nuclear material by macrophages. Lymph node sections from *gld* and *gld.apoE*$^{-/-}$ mice displayed reduced frequencies of macrophages with evidence of ingested TUNEL-positive material compared with wild-type or *apoE*$^{-/-}$ mice (Fig. 7, a and b). However, the decrease in frequency of macrophages with engulfed apoptotic nuclei was most evident in *gld.apoE*$^{-/-}$ mice ($P < 0.05$ relative to *gld*) (Fig. 7 c). Of note, the uptake of apoptotic nuclei by macrophages in *gld.apoE*$^{-/-}$ mice was significantly reduced when animals were fed Western diet compared with normal diet ($P < 0.05$). Therefore, lymph nodes from *gld.apoE*$^{-/-}$ mice displayed greater accumulation of apoptotic debris, whereas macrophages in these mice displayed a greater deficit in their ability to engulf this material, and both of these effects were more pronounced by a high cholesterol diet.

LPC Infusion Impairs Apoptotic Cell Clearance. LPC is the predominant phospholipid component of oxLDL that is believed to mediate many of the proatherogenic activities associated with hyperlipidemia (34). To test whether LPC could interfere with the clearance of apoptotic bodies, wild-type and *gld* mice were infused with LPC, and apoptotic material accumulation in lymph nodes was assessed (Fig. 8). For this experiment, two doses of LPC were chosen that are known to have vasoactive properties in vivo (35). LPC infusion led to a small, dose-dependent increase in the frequency of TUNEL-positive fragments in lymph nodes of wild-type mice. In contrast, infusion of LPC in *gld* mice led to markedly greater accumulation of apoptotic debris in lymph nodes. The level of apoptotic debris in lymph nodes from *gld* mice infused with LPC was similar to that seen in *gld.apoE*$^{-/-}$ mice fed Western diet (Fig. 6).

Discussion

Although it is widely accepted that inflammation plays a role in atherosclerosis, the etiology of accelerated atherosclerosis associated with autoimmune disease is not well understood. In this work, a mouse model was created by crossing a strain that is susceptible to atherosclerotic lesion formation (*apoE*$^{-/-}$) with a strain that develops lymphoproliferation and autoimmunity (*gld*). The *gld.apoE*$^{-/-}$ mice displayed threefold more atherosclerotic lesion area in the aorta than their *apoE*$^{-/-}$ counterparts on a Western diet. Surprisingly, the *gld.apoE*$^{-/-}$ mice exhibited exacerbated lymphoproliferation and autoimmunity relative to the *gld* phenotype, an effect that was further enhanced by Western diet. These data demonstrate synergistic interactions between the pathogenesis of atherosclerotic and autoimmune/lymphoproliferative diseases in the *gld.apoE*$^{-/-}$ mouse.

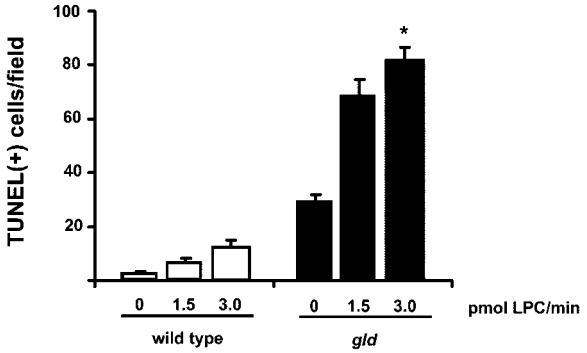

Figure 8. LPC promotes apoptotic body accumulation. LPC solutions or saline were infused for 120 min via tail vein in wild-type or *gld* mice. Lymph node sections were stained for TUNEL-positive cells. Quantified results reveal a significant increase in TUNEL-positive cells in *gld* mice after receiving LPC infusion (*, $P < 0.001$).

The role of Fas-mediated apoptosis in the genesis of vascular lesions is incompletely understood and controversial (36). Deficiencies in Fas-mediated apoptosis will produce vasculitis in some strains of mice (37) and promote intimal hyperplasia in a flow-restricted model of vascular injury (38). These data suggest that the Fas/FasL system is atheroprotective through its ability to inhibit vascular inflammation. However, acute overexpression of FasL or downstream effector molecules in wild-type animals was found to activate a proinflammatory program and promote atherosclerosis in some studies (39, 40), but not others (41, 42). The results of the current analysis show that, in toto, the Fas/FasL system has an atheroprotective function and that it serves to minimize vascular inflammation. In the context of the *apoE*$^{-/-}$ background, a deficiency in Fas-mediated apoptosis led to larger and more complex lesions, containing increased amounts of inflammatory cells and apoptotic debris. These features, in combination with the autoimmune phenotype, make the *gld.apoE*$^{-/-}$ mouse strain a relevant model system to study the pathophysiology of accelerated atherosclerosis that occurs in patients with autoimmune disease (13–15).

The *gld.apoE*$^{-/-}$ mice displayed increases in lymphadenopathy, splenomegaly, and autoimmune antibodies against cardiolipin and nuclear antigens compared with *gld* mice. The *gld.apoE*$^{-/-}$ mice also exhibited immune-mediated glomerular injury. In this mouse model, abnormal glomeruli and increased urinary protein excretion rates were observed. This is of particular interest because the strain of *gld* mouse (B6) that was used in this work does not normally exhibit appreciable renal dysfunction (43).

The interrelationship between vascular and autoimmune diseases in this mouse model may be mediated by perturbations in the mechanisms that clear apoptotic bodies. Recent studies in patients with SLE and lupus-prone animal models suggest that autoimmunity can result from defects in the ability to scavenge apoptotic bodies (3, 8). A key finding of our analysis is the observation that *gld.apoE*$^{-/-}$ mice contain significantly more TUNEL-positive nuclear fragments in their lymph nodes and higher levels of circulating apoptotic microparticles than the *gld* mice, consistent with the aggravated autoimmune phenotype in these animals. Despite these increases in apoptotic material, macrophages in *gld.apoE*$^{-/-}$ mice contained less apoptotic debris. The accumulation of apoptotic cells is of significance because delays in clearance will allow cells to enter late stages of apoptosis and secondary necrosis, and thereby promote inflammation (44). In addition, autoantigens become available for uptake by dendritic cells (2, 8). This process can facilitate the breakdown of peripheral tolerance through the effective presentation of autoantigens to the immune system.

The impaired clearance of apoptotic bodies may also have consequences for atherosclerotic disease. Patients with acute coronary syndromes have elevated levels of circulating apoptotic microparticles (29). These particles are highly thrombogenic and can account for the majority of the tissue factor activity in the lipid core of vascular plaques (45). In this regard, apoptotic fragments were found to be more abundant in the sera and atherosclerotic plaques of the *gld.apoE*$^{-/-}$ mice than the *apoE*$^{-/-}$ mice, and their accumulation in the vessel wall could contribute to lesion progression. In addition, aCL was markedly elevated in the *gld.apoE*$^{-/-}$ mice compared with *gld* or *apoE*$^{-/-}$ mice. aCL is a marker of autoimmune diseases and a risk factor for atherosclerosis and vascular complications (46, 47). Antiphospholipid antibodies may promote vascular inflammation by binding to apoptotic cells, thereby enabling their recognition by macrophage Fc receptors (48). Although macrophage phagocytosis of apoptotic bodies through scavenger receptors is normally antiinflammatory, uptake through Fc receptors can promote a proinflammatory state that is associated with cytokine secretion (48). Finally, immune complexes containing cardiolipin and other autoantigens can directly trigger endothelial cell expression of inflammatory cytokines and surface adhesion molecules, leading to endothelial dysfunction and their conversion to a prothrombotic phenotype (49).

It is interesting to speculate on how the process of atherogenesis can promote the accumulation of apoptotic bodies. OxLDL is a proatherogenic component of LDL cholesterol. OxLDL and antibodies against oxLDL can interfere with the recognition of the phosphatidylcholine moieties on apoptotic bodies by macrophage scavenger receptors and inhibit their phagocytosis (50, 51). Thus, the accumulation of apoptotic bodies in *gld.apoE*$^{-/-}$ mice could result from oxLDL-mediated interference of macrophage function. Consistent with this hypothesis is the observation that *gld.apoE*$^{-/-}$ mice maintained on Western versus normal diet displayed higher levels of apoptotic bodies in lymph nodes and a lower frequency of macrophages with ingested apoptotic debris. Furthermore, Western diet also increased circulating autoantibody levels as well as lymphadenopathy and splenomegaly. In this regard, we found that the continuous infusion of LPC, a major component of oxLDL, impairs apoptotic cell clearance. Although these effects could be seen in wild-type mice, the effects of LPC on apoptotic cell clearance were much more robust in *gld* mice. Recent data have suggested that LPC is a component of the phagocyte recruitment signals that are secreted by cells undergoing apoptosis (52). Therefore, high levels of LPC in hypercholesterolemic *gld.apoE*$^{-/-}$ mice might interfere with signal gradients that are required for the normal recruitment of phagocytes to dying cells.

In summary, the *gld.apoE*$^{-/-}$ model reflects the accelerated atherosclerosis that occurs in patients with autoimmune disorders. These data suggest that the immune dysregulation associated with SLE and similar disorders plays a key role in promoting atherogenesis. Our findings also indicate a positive feedback interaction between atherogenesis and autoimmune disease. In this regard, hyperlipidemic conditions may contribute to the severity of autoimmune disease by promoting the accumulation of apoptotic debris. Although it is difficult to ascertain the relationship between serum lipid levels and disease severity in patient populations

due to the prevalence of corticosteroid therapy, an analysis of untreated pediatric SLE patients concluded that hyperlipidemia was associated with the active disease (53). Furthermore, it has recently been reported that a cholesterol-lowering diet improves quality of life in patients with SLE (54). Therefore, further application of the *gld.apoE*$^{-/-}$ model could be valuable in delineating the interplay between autoimmunity and vascular disease progression.

The authors thank R. Smith, R. Pola, V. Zannis, and M. Sata for helpful advice. V. Zannis also provided advice and technical support for the measurement of circulating cholesterol levels. We also thank C. Broughton and M. Boulé for help with flow cytometry.

This work was supported by National Institutes of Health grants AG15052, AR40197, and AG17241 to K. Walsh, and by the National Kidney Foundation Clinical Scientist Award and National Institutes of Health grant DK02597 to I. Rifkin.

Submitted: 10 September 2003
Accepted: 4 March 2004

References

1. Kotzin, B.L. 1996. Systemic lupus erythematosus. *Cell.* 85: 303–306.
2. Savill, J., I. Dransfield, C. Gregory, and C. Haslett. 2002. A blast from the past: clearance of apoptotic cells regulates immune responses. *Nat. Rev. Immunol.* 2:965–975.
3. Potter, P.K., J. Cortes-Hernandez, P. Quartier, M. Botto, and M.J. Walport. 2003. Lupus-prone mice have an abnormal response to thioglycolate and an impaired clearance of apoptotic cells. *J. Immunol.* 170:3223–3232.
4. Taylor, P.R., A. Carugati, V.A. Fadok, H.T. Cook, M. Andrews, M.C. Carroll, J.S. Savill, P.M. Henson, M. Botto, and M.J. Walport. 2000. A hierarchical role for classical pathway complement proteins in the clearance of apoptotic cells in vivo. *J. Exp. Med.* 192:359–366.
5. Yasutomo, K., T. Horiuchi, S. Kagami, H. Tsukamoto, C. Hashimura, M. Urushihara, and Y. Kuroda. 2001. Mutation of DNASE1 in people with systemic lupus erythematosus. *Nat. Genet.* 28:313–314.
6. Rumore, P.M., and C.R. Steinman. 1990. Endogenous circulating DNA in systemic lupus erythematosus. Occurrence as multimeric complexes bound to histone. *J. Clin. Invest.* 86: 69–74.
7. Williams, R.C., Jr., C.C. Malone, C. Meyers, P. Decker, and S. Muller. 2001. Detection of nucleosome particles in serum and plasma from patients with systemic lupus erythematosus using monoclonal antibody 4H7. *J. Rheumatol.* 28:81–94.
8. Baumann, I., W. Kolowos, R.E. Voll, B. Manger, U. Gaipl, W.L. Neuhuber, T. Kirchner, J.R. Kalden, and M. Herrmann. 2002. Impaired uptake of apoptotic cells into tingible body macrophages in germinal centers of patients with systemic lupus erythematosus. *Arthritis Rheum.* 46:191–201.
9. Ross, R. 1999. Atherosclerosis--an inflammatory disease. *N. Engl. J. Med.* 340:115–126.
10. Binder, C.J., M.K. Chang, P.X. Shaw, Y.I. Miller, K. Hartvigsen, A. Dewan, and J.L. Witztum. 2002. Innate and acquired immunity in atherogenesis. *Nat. Med.* 8:1218–1226.
11. Manzi, S., E.N. Meilahn, J.E. Rairie, C.G. Conte, T.A.J. Medsger, L. Jansen-McWilliams, R.B. D'Agostino, and L.H. Kuller. 1997. Age-specific incidence rates of myocardial infarction and angina in women with systemic lupus erythematosus: comparison with the Framingham study. *Am. J. Epidemiol.* 145:408–415.
12. Urowitz, M.B., A.A. Bookman, B.E. Koehler, D.A. Gordon, H.A. Smythe, and M.A. Ogryzlo. 1976. The bimodal mortality pattern of systemic lupus erythematosus. *Am. J. Med.* 60:221–225.
13. Lockshin, M.D., J.E. Salmon, and M.J. Roman. 2001. Atherosclerosis and lupus: a work in progress. *Arthritis Rheum.* 44:2215–2217.
14. Van Doornum, S., G. McColl, and I.P. Wicks. 2002. Accelerated atherosclerosis: an extraarticular feature of rheumatoid arthritis? *Arthritis Rheum.* 46:862–873.
15. Riboldi, P., M. Gerosa, C. Luzzana, and L. Catelli. 2002. Cardiac involvement in systemic autoimmune diseases. *Clin. Rev. Allergy Immunol.* 23:247–261.
16. Nagata, S., and P. Golstein. 1995. The Fas death factor. *Science.* 267:1449–1456.
17. Krammer, P.H., I. Behrmann, P. Daniel, J. Dhein, and K.M. Debatin. 1994. Regulation of apoptosis in the immune system. *Curr. Opin. Immunol.* 6:279–289.
18. Ashany, D., X. Song, E. Lacy, J. Nikolic-Zugic, S.M. Friedman, and K.B. Elkon. 1995. Th1 CD4+ lymphocytes delete activated macrophages through the Fas/APO-1 antigen pathway. *Proc. Natl. Acad. Sci. USA.* 92:11225–11229.
19. Perlman, H., L.J. Pagliari, C. Georganas, T. Mano, K. Walsh, and R.M. Pope. 1999. FLICE-inhibitory protein expression during macrophage differentiation confers resistance to Fas-mediated apoptosis. *J. Exp. Med.* 190:1679–1688.
20. Fisher, G.H., F.J. Rosenberg, S.E. Straus, J.K. Dale, L.A. Middelton, A.Y. Lin, W. Strober, M.J. Lenardo, and J.M. Puck. 1995. Dominant interfering Fas gene mutations impair apoptosis in a human autoimmune lymphoproliferative syndrome. *Cell.* 81:935–946.
21. Rieux-Laucat, F., F. LeDeist, C. Hivroz, I.A.G. Roberts, K.M. Debatin, A. Fischer, and J.P. deVillartay. 1995. Mutations in Fas associated with human lymphoproliferatie syndrome and autoimmunity. *Science.* 268:1347–1349.
22. Drappa, J., A.K. Vaishnaw, K.E. Sullivan, J.L. Chu, and K.B. Elkon. 1996. *Fas* gene mutations in the Canale-Smith syndrome, an inherited lymphoproliferative disorder associated with autoimmunity. *N. Engl. J. Med.* 335:1643–1649.
23. Takahashi, T., M. Tanaka, C.I. Brannan, N.A. Jenkins, N.G. Copeland, T. Suda, and S. Nagata. 1994. Generalized lymphoproliferative disease in mice, caused by a point mutation in the Fas ligand. *Cell.* 76:969–976.
24. Roths, J.B., E.D. Murphy, and E.M. Eicher. 1984. A new mutation, *gld*, that produces lymphoproliferation and autoimmunity in C3H/HeJ mice. *J. Exp. Med.* 159:1–20.
25. Nagata, S. 1998. Human autoimmune lymphoproliferative syndrome, a defect in the apoptosis-inducing Fas receptor: a lesson from the mouse model. *J. Hum. Genet.* 43:2–8.
26. Cohen, P.L., and R.A. Eisenberg. 1991. Lpr and gld: single gene models of systemic autoimmunity and lymphoproliferative disease. *Annu. Rev. Immunol.* 9:243–269.
27. Qiao, J.H., L.W. Castellani, M.C. Fishbein, and A.J. Lusis. 1993. Immune-complex-mediated vasculitis increases coronary artery lipid accumulation in autoimmune-prone MRL mice. *Arterioscler. Thromb.* 13:932–943.
28. Meyer, T.W., and H.G. Rennke. 1988. Increased single-nephron protein excretion after renal ablation in nephrotic rats. *Am. J. Physiol.* 255:F1243–F1248.
29. Mallat, Z., H. Benamer, B. Hugel, J. Benessiano, P.G. Steg,

J.M. Freyssinet, and A. Tedgui. 2000. Elevated levels of shed membrane microparticles with procoagulant potential in the peripheral circulating blood of patients with acute coronary syndromes. *Circulation*. 101:841–843.
30. Plump, A.S., J.D. Smith, T. Hayek, K. Aalto-Setälä, A. Walsh, J.G. Verstuyft, E.M. Rubin, and J.L. Breslow. 1992. Severe hypercholesterolemia and atherosclerosis in apolipoprotein E-deficient mice created by homologous recombination in ES cells. *Cell*. 71:343–353.
31. Harada, K., Z. Chen, S. Ishibashi, J. Osuga, H. Yagyu, K. Ohashi, N. Yahagi, F. Shionoiri, L. Sun, Y. Yazaki, and N. Yamada. 1997. Apoptotic cell death in atherosclerotic plaques of hyperlipidemic knockout mice. *Atherosclerosis*. 135:235–239.
32. Bleesing, J.J., M.R. Brown, C. Novicio, D. Guarraia, J.K. Dale, S.E. Straus, and T.A. Fleisher. 2002. A composite picture of TcR alpha/beta(+) CD4(-)CD8(-) T cells (alpha/beta-DNTCs) in humans with autoimmune lymphoproliferative syndrome. *Clin. Immunol*. 104:21–30.
33. Horkko, S., E. Miller, E. Dudl, P. Reaven, L.K. Curtiss, N.J. Zvaifler, R. Terkeltaub, S.S. Pierangeli, D.W. Branch, W. Palinski, and J.L. Witztum. 1996. Antiphospholipid antibodies are directed against epitopes of oxidized phospholipids. Recognition of cardiolipin by monoclonal antibodies to epitopes of oxidized low density lipoprotein. *J. Clin. Invest*. 98:815–825.
34. Ross, R. 1993. The pathogenesis of atherosclerosis: a perspective for the 1990s. *Nature*. 362:801–809.
35. Handa, R.K., and V.M. Buckalew, Jr. 1992. Effect of lysophosphatidylcholine on renal hemodynamics and excretory function in anesthetized rats. *Life Sci*. 51:1571–1575.
36. Walsh, K., R.C. Smith, and H.S. Kim. 2000. Vascular cell apoptosis in remodeling, restenosis and plaque rupture. *Circ. Res*. 87:184–188.
37. Hewicker, M., and G. Trautwein. 1987. Sequential study of vasculitis in MRL mice. *Lab. Anim*. 21:335–341.
38. Sata, M., and K. Walsh. 2000. Fas ligand-deficient mice display enhanced leukocyte infiltration and intima hyperplasia in flow-restricted vessels. *J. Mol. Cell. Cardiol*. 32:1395–1400.
39. Schneider, D.B., G. Vassalli, S. Wen, R.M. Driscoll, A.B. Sassani, M.B. DeYoung, R. Linnemann, R. Virmani, and D.A. Dichek. 2000. Expression of Fas ligand in arteries of hypercholesterolemic rabbits accelerates atherosclerotic lesion formation. *Arterioscler. Thromb. Vasc. Biol*. 20:298–308.
40. Schaub, F.J., D.K. Han, W.C. Liles, L.D. Adams, S.A. Coats, R.K. Ramachandran, R.A. Seifert, S.M. Schwartz, and D.F. Bowen-Pope. 2000. Fas/FADD-mediated activation of a specific program of inflammatory gene expression in vascular smooth muscle cells. *Nat. Med*. 6:790–796.
41. Sata, M., H. Perlman, D.A. Muruve, M. Silver, M. Ikebe, T.A. Libermann, P. Oettgen, and K. Walsh. 1998. Fas ligand gene transfer to the vessel wall inhibits neointima formation and overrides the adenovirus-mediated T cell response. *Proc. Natl. Acad. Sci. USA*. 95:1213–1217.
42. Luo, Z., M. Sata, T. Nguyen, J.M. Kaplan, G.Y. Akita, and K. Walsh. 1999. Adenovirus-mediated delivery of Fas ligand inhibits intimal hyperplasia after balloon injury in immunologically primed animals. *Circulation*. 99:1776–1779.
43. Kelley, V.E., and J.B. Roths. 1985. Interaction of mutant Ipr gene with background strain influences renal disease. *Clin. Immunol. Immunopathol*. 37:220–229.
44. Gaipl, U.S., J. Brunner, T.D. Beyer, R.E. Voll, J.R. Kalden, and M. Herrmann. 2003. Disposal of dying cells: a balancing act between infection and autoimmunity. *Arthritis Rheum*. 48: 6–11.
45. Mallat, Z., B. Hugel, J. Ohan, G. Leseche, J.M. Freyssinet, and A. Tedgui. 1999. Shed membrane microparticles with procoagulant potential in human atherosclerotic plaques: a role for apoptosis in plaque thrombogenicity. *Circulation*. 99: 348–353.
46. Ahmed, E., S. Nityanand, A. Mustafa, K. Brismar, and A.K. Lefvert. 1999. Anti-cardiolipin antibodies and circulating immune complexes in type 1 diabetes mellitus: increased prevalence and relation to vascular complications. *Clin. Exp. Immunol*. 115:255–259.
47. Vaarala, O. 2000. Autoantibodies to modified LDLs and other phospholipid-protein complexes as markers of cardiovascular diseases. *J. Intern. Med*. 247:381–384.
48. Manfredi, A.A., P. Rovere, G. Galati, S. Heltai, E. Bozzolo, L. Soldini, J. Davoust, G. Balestrieri, A. Tincani, and M.G. Sabbadini. 1998. Apoptotic cell clearance in systemic lupus erythematosus. I. Opsonization by antiphospholipid antibodies. *Arthritis Rheum*. 41:205–214.
49. Sundy, J.S., and B.F. Haynes. 2000. Cytokines and adhesion molecules in the pathogenesis of vasculitis. *Curr. Rheumatol. Rep*. 2:402–410.
50. Sambrano, G.R., and D. Steinberg. 1995. Recognition of oxidatively damaged and apoptotic cells by an oxidized low density lipoprotein receptor on mouse peritoneal macrophages: role of membrane phosphatidylserine. *Proc. Natl. Acad. Sci. USA*. 92:1396–1400.
51. Chang, M.K., C. Bergmark, A. Laurila, S. Horkko, K.H. Han, P. Friedman, E.A. Dennis, and J.L. Witztum. 1999. Monoclonal antibodies against oxidized low-density lipoprotein bind to apoptotic cells and inhibit their phagocytosis by elicited macrophages: evidence that oxidation-specific epitopes mediate macrophage recognition. *Proc. Natl. Acad. Sci. USA*. 96:6353–6358.
52. Lauber, K., E. Bohn, S.M. Krober, Y.J. Xiao, S.G. Blumenthal, R.K. Lindemann, P. Marini, C. Wiedig, A. Zobywalski, S. Baksh, et al. 2003. Apoptotic cells induce migration of phagocytes via caspase-3-mediated release of a lipid attraction signal. *Cell*. 113:717–730.
53. Ilowite, N.T., P. Samuel, E. Ginzler, and M.S. Jacobson. 1988. Dyslipoproteinemia in pediatric systemic lupus erythematosus. *Arthritis Rheum*. 31:859–863.
54. Shah, M., A. Kavanaugh, Y. Coyle, B. Adams-Huet, and P.E. Lipsky. 2002. Effect of a culturally sensitive cholesterol lowering diet program on lipid and lipoproteins, body weight, nutrient intakes, and quality of life in patients with systemic lupus erythematosus. *J. Rheumatol*. 29:2122–2128.